Ceramics International 43 (2017) 11627–11634

Contents lists available at ScienceDirect

Ceramics International

journal homepage: www.elsevier.com/locate/ceramint

Effects of creep-plastic behavior on stress development in TBCs during cooling

Yijun Chai, Chen Lin, Yueming Li*

State Key Laboratory for Strength and Vibration of Mechanical Structures, Shaanxi Key Laboratory of Environment and Control for Flight Vehicle, Xi'an Jiaotong University, No. 28 Xianning West Road, Xi'an 710049, China

ARTICLE INFO

Keywords:
Creep-plastic behavior
Stress development
Interface roughness
Cooling rate
Thermal barrier coatings

ABSTRACT

The stress development, as the main cause of TBCs failure, can be significantly influenced by the non-linear behaviors of TBCs materials (e.g. plastic and creep deformations). Description of the non-linear behaviors of TBCs materials is crucial to accurate stress evaluation. However, conventional constitutive models couldn't distinguish the role of the nonlinear plastic and creep deformations in the stress evaluation, which may lead to obvious difference. This work employs the creep-plastic constitutive model to study the effects of creep-plastic behavior of BC and TGO on the TC/TGO/BC interface stress development. This creep-plastic model reveals that the stress can be identified in three sections when BC creep properties varies in wide margins: In the first section with a small BC creep rate, plastic deformation mainly influences the interface stresses; in the second section with a medium creep rate, both creep and plastic deformations affect the stress development; in the third section with a larger creep rate, creep becomes the main factor dominating the relaxing process. It is also found that if the creep in TGO is considered, the stresses will be overall relaxed no matter if BC is plastic, creep or creep-plastic. Based on this three-section phenomenon, the influence of TGO thickness, interface roughness and cooling rate on the stress development is investigated.

1. Introduction

Thermal barrier coatings (TBCs) are refractory, anti-oxidation and corrosion resistance, mainly applied on gas turbine engines hottest parts. Extreme high-temperature gas in aggressive thermo-mechanical environments can then be isolated from the core metallic engine parts, allowing them to operate at higher temperatures above their melting points to maximize the efficiency and prolong the service life [1,2]. A typical structure of TBCs consists of three layers. The outer layer is TC (top coat) composed of 7 wt% Y_2O_3-stabilized ZrO_2 (7YSZ) ceramics with low thermal conductivity, which makes it a main structure isolating the external high temperature. The inner layer is BC (bond coat) made of MCrAlY superalloy, improving the adherence between TC and substrate. Under the heat operating conditions, oxidation takes place in BC with oxygen diffusing through TC, and a thin film - TGO (thermally grown oxide) forms between BC and TC [3,4]. These multifunctional layers compose a TBC system. Spallation of TBCs during service process can expose the engine hottest parts into the extremely high temperature, oxidation and corrosion environment, which can jeopardize the engine's working condition. Thus, it is of significance to study the failure mechanisms of TBCs. However, due to the complex structure of TBCs and the markedly different physical, thermal and mechanical properties of these layers, there are more difficulties in studying on TBCs [5,6].

The stress development, which is one of the main causes of TBCs failure, can be influenced by various factors. (1) Oxidation at elevated temperatures can induce considerable compressive growth stress in TGO [7–11], and can shift the final stress state between compressive and tensile [12,13], promoting crack formation. (2) High temperature sintering of TC in air plasma sprayed (APS) TBCs could increase its thermal conductivity coefficient and the Young's module [14–16], which could lead to the poor performance of heat insulation and a higher TC stress level. (3) The thermal mismatch between different layers can induce deformation compatibility among TC, TGO and BC layers [9,13,17,18]. The compressive stress in TGO layer can then become larger, which enhances the out-of-plane displacement of TGO. As a result, significant change in the stress magnitude in TBCs can be observed during the cooling stage. (4) The non-linear behaviors of TBCs materials during thermal cycling have a strong impact on the stress development. Various constitutive models have been applied for stress evaluation in previous researches to describe the non-linear behaviors [19–23]. However, they cannot distinguish the role of the

* Corresponding author.
E-mail address: liyueming@mail.xjtu.edu.cn (Y. Li).

http://dx.doi.org/10.1016/j.ceramint.2017.05.338
Received 21 March 2017; Received in revised form 10 May 2017; Accepted 29 May 2017
Available online 30 May 2017

nonlinear plastic and creep deformations in the stress evaluation, which gives obviously difference. Since governed by different mechanisms [24], creep and plastic deformations can simultaneously develop at suitable stress levels. Meanwhile, it is noted that the creep and plastic deformations of TBCs materials can be also affected by extreme thermal cycling [25]. The accurate description of the non-linear behaviors of TBCs materials would be crucial in stress evaluation, to reveal how the creep and plastic deformations evolve and how they affect the stress development.

This work aims at studying the evolution of creep and plastic deformation with mechanical properties variations and the effects of creep-plastic behavior on the stress development. The TGO growth, the geometry morphology and the environment condition which have a strong impact on the stress development are also discussed in this work. A typical service process consisting of a heating stage for 300 h and a cooling stage for 120 s is considered. Based on a stress-free state at the end of the heating stage, the cooling stresses are emphatically discussed. The paper is organized as follows. In Part 2, a creep-plastic constitutive model is introduced. A finite element model with a sinusoidal interface is presented in Part 3. In Part 4, the effects of the creep-plastic behavior on the interface stresses with variation of creep properties are investigated, and the effects of the TGO thickness, the interface roughness as well as the cooling rate on the stress development are studied. The conclusions are stated in Part 5. The results in this paper may help to understand the evolution of creep and plastic deformations for better stress predication, and could provide reference to optimize TBCs materials.

2. Theoretical models

2.1. Diffusion-oxidation reaction model for the TGO layer

During a long-term service under high temperature, material in BC layer is gradually oxidized to TGO as oxygen diffuses through the TC layer. Thus, there is a thin layer appearing at the interface where both the BC and TGO materials co-exist, which is defined as a transient oxidation front. In this study, a diffusion-oxidation reaction model proposed in our previous work [26] is employed to describe the TGO growth, which can consider the continuous oxygen consumption effect in the formation of TGO during heating:

$$\dot{c}_{O^{2-}} = D\mathrm{div}(\nabla c_{O^{2-}}) - \kappa\dot{\xi} \tag{1}$$

where $c_{O^{2-}}$ is the distribution of concentration of oxygen anion; div is the divergence operator and ∇ is the gradient operator; κ is the amount of oxygen consumed per unit reference volume during oxidation. $\dot{\xi}$ is the changing rate of the TGO dimensionless molar fraction ξ, which can be expressed as:

$$\dot{\xi} = \gamma(1-\xi)c_{O^{2-}} \tag{2}$$

and D in Eq. (1) is the oxygen diffusion coefficient:

$$D = \xi D_{\mathrm{TGO}} + (1-\xi)D_{\mathrm{BC}} \tag{3}$$

where D_{TGO} and D_{BC} are the oxygen diffusion coefficients of TGO and BC respectively.

2.2. The creep-plastic constitutive model

To consider the plastic and creep behaviors of material simultaneously, a creep-plastic constitutive model proposed in our previous work [26] is introduced to characterize the deformation behaviors of the TGO and BC:

$$\boldsymbol{\sigma}_{\mathrm{TGO}} = \mathbf{D}^{\mathrm{e}}_{\mathrm{TGO}}: (\boldsymbol{\varepsilon}_{\mathrm{TGO}} - \boldsymbol{\varepsilon}^{\mathrm{th}}_{\mathrm{TGO}} - \boldsymbol{\varepsilon}^{\mathrm{g}}_{\mathrm{TGO}} - \boldsymbol{\varepsilon}^{\mathrm{p}}_{\mathrm{TGO}} - \boldsymbol{\varepsilon}^{\mathrm{c}}_{\mathrm{TGO}}) \tag{4}$$

$$\boldsymbol{\sigma}_{\mathrm{BC}} = \mathbf{D}^{\mathrm{e}}_{\mathrm{BC}}: (\boldsymbol{\varepsilon}_{\mathrm{BC}} - \boldsymbol{\varepsilon}^{\mathrm{th}}_{\mathrm{BC}} - \boldsymbol{\varepsilon}^{\mathrm{p}}_{\mathrm{BC}} - \boldsymbol{\varepsilon}^{\mathrm{c}}_{\mathrm{BC}}) \tag{5}$$

where $\mathbf{D}^{\mathrm{e}}$ is the elastic stiffness matrix; $\boldsymbol{\varepsilon}$ is the total strain; $\varepsilon^{\mathrm{th}}$ is the thermal strain, which can be obtained by the following equations:

$$\boldsymbol{\varepsilon}^{\mathrm{th}}_{\mathrm{TGO}} = \alpha_{\mathrm{TGO}}(T - T_{ref})\mathbf{i} \tag{6}$$

$$\boldsymbol{\varepsilon}^{\mathrm{th}}_{\mathrm{BC}} = \alpha_{\mathrm{BC}}(T - T_{ref})\mathbf{i} \tag{7}$$

where α is the thermal expansion coefficient; T_{ref} is the reference temperature valuing 1100 °C; $\mathbf{i} = [1, 1, 1, 0, 0, 0]^{\mathrm{T}}$ is a vector.
$\boldsymbol{\varepsilon}^{\mathrm{g}}_{\mathrm{TGO}}$ is the permanent volumetric swelling strain of the TGO [27]:

$$\boldsymbol{\varepsilon}^{\mathrm{g}}_{\mathrm{TGO}} = \varepsilon^{\mathrm{g}}_{\mathrm{v}}\mathbf{i} \tag{8}$$

where $\varepsilon^{\mathrm{g}}_{\mathrm{v}} = 0.08$ is the mean swelling strain derived from Pilling-Bedworth ratio.
$\boldsymbol{\varepsilon}^{\mathrm{p}}$ is the plastic strain obtained based on the plastic flow rule. $\boldsymbol{\varepsilon}^{\mathrm{c}}$ is the creep strain. The following Norton power-law creep behavior is used [28]:

$$\dot{\bar{\varepsilon}}^{\mathrm{c}}_{\mathrm{TGO}} = \mathrm{A}_{\mathrm{TGO}}\exp\left[-\frac{Q_{\mathrm{TGO}}}{\mathrm{R}(\mathrm{T}+273)}\right][q(\boldsymbol{\sigma}_{\mathrm{TGO}})]^{n_{\mathrm{TGO}}} \tag{9}$$

$$\dot{\bar{\varepsilon}}^{\mathrm{c}}_{\mathrm{BC}} = \mathrm{A}_{\mathrm{BC}}\exp\left[-\frac{Q_{\mathrm{BC}}}{\mathrm{R}(\mathrm{T}+273)}\right][q(\boldsymbol{\sigma}_{\mathrm{BC}})]^{n_{\mathrm{BC}}} \tag{10}$$

here $\dot{\bar{\varepsilon}}$ is the equivalent creep rate; A, Q, R, T,n are the reference creep strain rate, the activation energy for creep, the gas constant (R = 8.314 J mol^{-1} K^{-1}), the Celsius temperature and the power-law creep exponent, respectively.

The effective constitutive behavior in the transient oxidation front (BC–TGO mixed zone) is modeled based on the Voigt's assumption [29]:

$$\boldsymbol{\varepsilon} = \boldsymbol{\varepsilon}_{\mathrm{TGO}} = \boldsymbol{\varepsilon}_{\mathrm{BC}} \tag{11}$$

$$\boldsymbol{\sigma} = \xi\boldsymbol{\sigma}_{\mathrm{TGO}} + (1-\xi)\boldsymbol{\sigma}_{\mathrm{BC}} \tag{12}$$

where $\boldsymbol{\varepsilon}$ is the total strain; $\boldsymbol{\sigma}$ is the effective stress in the mixture zone.

A return-mapping type algorithm is employed for the solution of the combined creep-plastic constitutive model [26].

3. Numerical analysis

This part introduces the numerical calculation conditions used in the finite element analysis, including detailed information of the TBCs finite element model, material parameters of the diffusion-oxidation reaction model and the constitutive equations.

3.1. Finite element model

For the present work, the TBCs consist of a MCrAlY oxidation-resistant BC, a YSZ TC deposited by APS, and a TGO composed of alumina which grows during heating. This coating system is bonded to a superalloy substrate. In this study, a two-dimensional four-node generalized plane strain finite element model with a periodic array of sinusoidal interface is applied, as illustrated in Fig. 1. Within the model, the TGO forms during the isothermal exposure period of 300 h at 1100 °C. Following the exposure, a cooling to 20 °C takes place within 120 s. The TBCs are considered to be stress-free at the initial stage of heating.

For the diffusion analysis, the oxygen anion concentration is assumed to be uniform on the interface between TC and BC, since the TC layer is commonly regarded to be fully transparent to oxygen. The value of oxygen anion concentration is considered to be 1.5 mol/m^3 [26].

The displacement boundary conditions are illustrated in Fig. 1. The axisymmetric boundary of the model is constrained in x_1 direction. The nodes on the bottom are free to move in x_1 direction but constrained in x_2 direction. The left TBCs surface is allowed to move in x_1 direction by a uniform displacement during cooling:

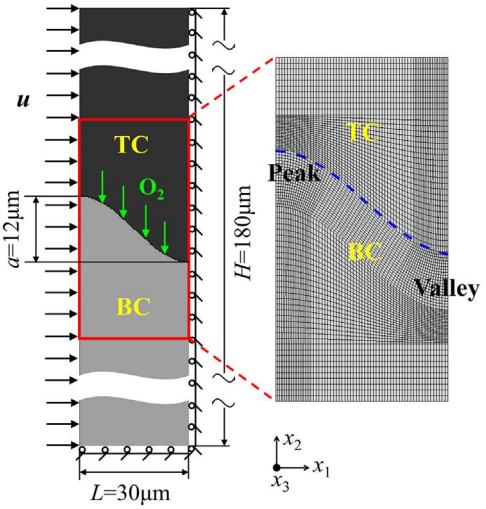

Fig. 1. Finite element model of TBCs.

$$u = \alpha_{sub}(T - T_{ref})L \quad (13)$$

where α_{sub} is the thermal mismatch coefficient of the substrate and L = 30 μm is the length of model shown in Fig. 1.

In the direction x_3 perpendicular to the x_1–x_2 plane, the deformation of the substrate is imposed on the TBCs by a generalized plane-strain condition:

$$\varepsilon_{33} = \alpha_{sub}(T - T_{ref}) \quad (14)$$

3.2. Physical and mechanical properties

In this study, all layers are considered to be isotropic. TC is assumed to be elastic, and the sintering effects are not taken into account. During heating, the BC and TGO are assumed to be combined creep-plastic materials to ensure a stress-free state. During cooling, two cases are studied to reveal the creep-plastic behavior: (1) BC is creep-plastic material while TGO elastic, and (2) both BC and TGO are creep-plastic materials.

Note that the material properties of the layers could change during the complex process (such as sintering, oxidation, phase transformation) in thermal cycling. It is then difficult to determine all the material parameters at different temperatures. Thus, a variation of BC creep properties is selected to simulate the effects of creep-plastic behavior here. The temperature-dependent material properties are listed in Table 1.

Table 2
The diffusion and oxidation parameters.

	Parameter	Value
Oxygen diffusion in TC	$D_{TC}/(m^2/s)$	∞
Oxygen diffusion in BC/TGO[13]	$D_{BC} = D_{TGO}/(m^2/s)$	3.5×10^{-14}
Reference value for the diffusion-oxidation model	$k^{32}/(mol/m^3)$	0.24×10^6
	$\gamma^9/(m^3/(mol \times s))$	1.25×10^{-4}

The parameters in the diffusion-oxidation reaction model in Eq. (1) are shown in Table 2. The values of oxygen diffusion coefficients of the TGO and BC phase are regarded to be the same [13]. The parameter κ obtained in [32] is used. The parameter γ in Eq. (2) can be numerically calculated via the process of TGO formation in the experiment [9].

4. Results and discussions

4.1. The effects of BC creep-plastic behavior on the stress development

In this part, the effects of BC creep-plastic behavior on the stress development are investigated, with creep rate in wide margins. The TBCs are considered to experience a 120 s cooling stage after exposed to 1100 °C for 300 h. The TGO, which is assumed to be elastic, grows to 6 μm after heating and has an interface roughness ratio of a/L = 0.4. The interface stresses upon cooling are analyzed. As the stress in x_2 direction is one of the main factors leading to the TBCs crack, this work aims at exploring the stress component σ_{22}.

The stress during cooling is mainly affected by both the thermal mismatch between the layers and the relaxation due to the creep and plastic deformations. Here, the stresses are evaluated by considering the BC to be elastic, perfect elasto-plastic, creep and creep-plastic behavior, respectively. The stresses at TC valley and peak, BC valley and peak (see Fig. 1) as well as the maximum tensile stress on TC/TGO interface are investigated.

Fig. 2(a) and (b) display that, when the BC is considered to be elastic, elasto-plastic and creep respectively, the stress development shows obvious difference. This implies the necessity of accurate description of the non-linear behaviors in stress evaluation. Based on this reason, the creep-plastic constitutive model mentioned above is employed in this work, to evaluate the stress development. It can be found that, when BC creep rate A_{BC} varies from 10^{-6} to 10^{-3} $MPa^{-4.1}$ s^{-1}, there is no difference of the stresses on the TC and BC interfaces between the elasto-plastic and creep-plastic assumptions, while the creep and creep-plastic assumptions exhibit significant

Table 1
The temperature dependent mechanics parameters [30,31].

T/°C		20	200	400	600	800	1000	1100
TC	E^{30}(GPa)	48	47	44	40	34	26	22
	ν^{30}	0.1	0.1	0.1	0.11	0.11	0.12	0.12
	$\alpha^{30}(10^{-6}/°C)$	9.7	9.8	9.9	9.9	10	10.1	10.1
BC	E^{30}(GPa)	200	190	175	160	145	120	110
	ν^{30}	0.3	0.3	0.31	0.31	0.32	0.33	0.33
	$\alpha^{30}(10^{-6}/°C)$	12.3	13.2	14.2	15.2	16.3	17.2	17.7
	$\sigma_{Y,BC}$(MPa)[26]	426	412	396	362	284	202	114
	$A_{BC}(MPa^{-n}\ s^{-1})$[26,31]	10^{-5}–10^6	–	–	–	–	–	6.31×10^{-6}
	n_{BC}[31]	4.09	4.09	4.09	4.09	4.09	4.09	2.2
	Q_{BC}(kJ/mol)[31]	263	263	263	263	263	263	165
TGO	E^{30}(GPa)	400	390	380	370	355	325	320
	ν^{30}	0.23	0.23	0.24	0.24	0.25	0.25	0.25
	$\alpha^{30}(10^{-6}/°C)$	8	8.2	8.4	8.7	9	9.3	9.5
	$\sigma_{Y,TGO}$(GPa)[26]	10	10	10	10	10	1	1
	$A_{TGO}(MPa^{-2.3}\ s^{-1})$[20]	$6.8 \times (10^8$–$10^{13})$	–	–	–	–	–	6.8×10^3
	n_{TGO}[20]	2.3	–	–	–	–	–	2.3
	Q_{TGO}(kJ/mol)[20]	424	–	–	–	–	–	424
Substrate	$\alpha^{30}(10^{-6}/°C)$	14.8	15.2	15.6	16.2	16.9	17.2	17.6

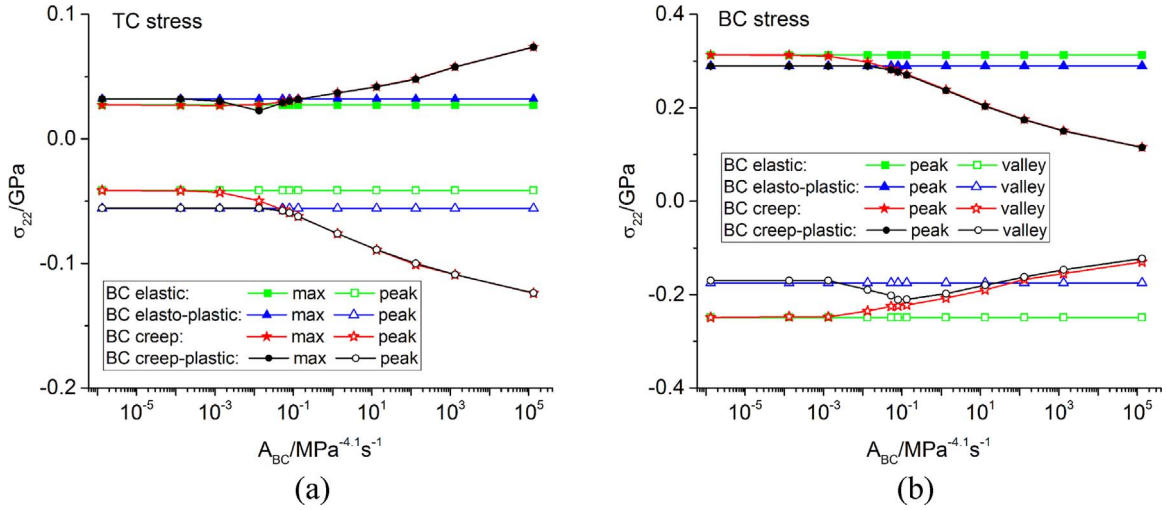

Fig. 2. Stress σ_{22} considering BC elastic, elasto-plastic, creep and creep-plastic behavior, respectively. (a) For the maximum stress and peak position on TC/TGO interface, (b) for the valley and peak positions on BC/TGO interface.

difference. Therefore, the plastic deformation is the main factor affecting the interface stresses in this section. With the BC creep rate constantly increasing from 10^{-3} to 10^{-1} $MPa^{-4.1}$ s^{-1}, the interface stresses obtained by these four assumptions are all different, indicating that both the creep and plastic behavior influence the stresses. With the BC creep rate ranging from 10^{-1} to 10^{5} $MPa^{-4.1}$ s^{-1}, it can be found that the creep rather than the plastic behavior affects the stress development. In total, with different creep properties, the main factors controlling the stress could be plastic, creep-plastic and creep deformation respectively. The effects of the creep properties have been studied by other researchers [22,26]; however, only one of these three phenomena was reported. In the following parts, the effects of the BC creep-plastic behavior on the stress development will be discussed in detail.

Fig. 3 shows the interface stresses σ_{22} by considering BC creep-plastic behavior with different creep rates. For cases where the BC exhibits different creep from very slow ($A_{BC} = 10^{-6}$ $MPa^{-4.1}$ s^{-1}) to fast ($A_{BC} = 10^{5}$ $MPa^{-4.1}$ s^{-1}), σ_{22} behaves in three evolution trends: Sections 1–3. Fig. 4 shows the equivalent plastic strain and the equivalent creep strain development, which clearly illustrates how these three sections are identified. Besides, three representative creep rates in these three sections (i.e., $A_{BC} = 10^{-4}$ $MPa^{-4.1}$ s^{-1}, $A_{BC} = 2\times10^{-4}$ $MPa^{-4.1}$ s^{-1}, $A_{BC} = 10^{2}$ $MPa^{-4.1}$ s^{-1}) are chosen respectively, and the time-dependent evolution with the three creep rates are evaluated (Fig. 5), to vividly show how the creep and plastic strain evolve during cooling. Detailed discussions are given below.

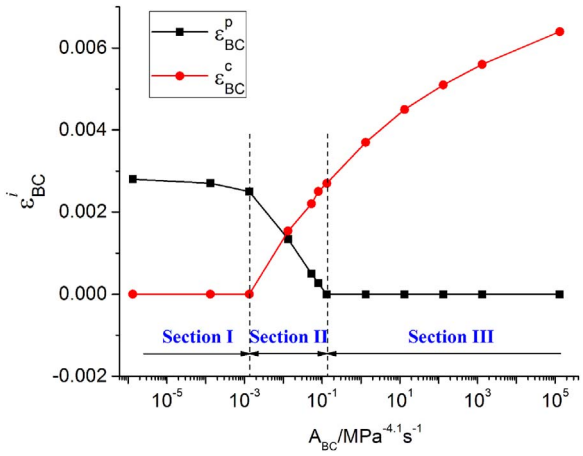

Fig. 4. Evolution of the maximum equivalent creep and plastic strain of BC for BC creep-plastic and TGO elastic.

Fig. 4 shows that in Section 1 with relatively smaller creep rates ($A_{BC} = 10^{-6}$–10^{-2} $MPa^{-4.1}$ s^{-1}), only plastic deformation occurs due to

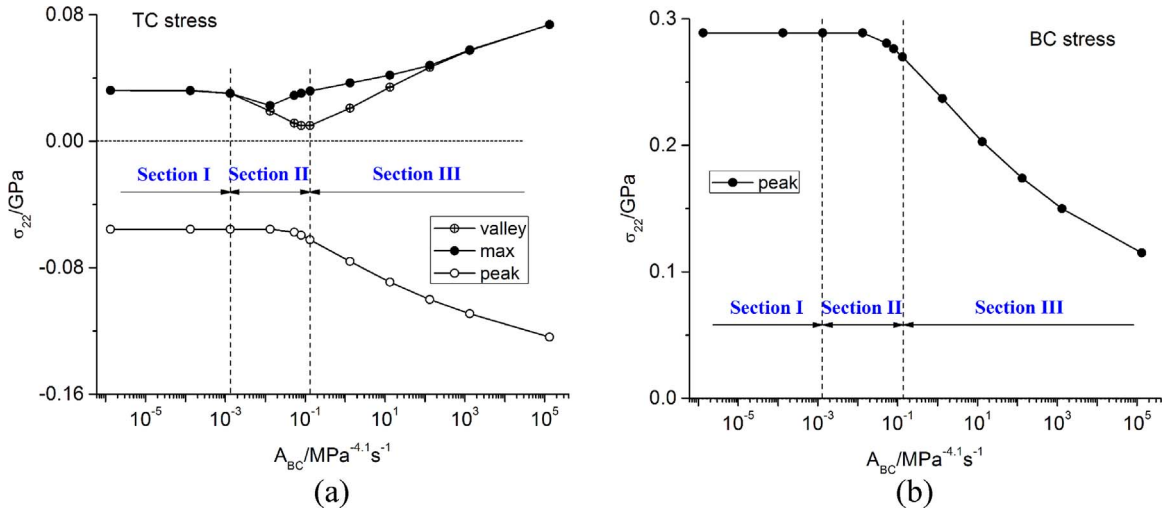

Fig. 3. Stress σ_{22} considering BC creep-plastic behavior. (a) For the maximum stress, the valley and peak positions on TC/TGO interface, (b) for the peak position on BC/TGO interface.

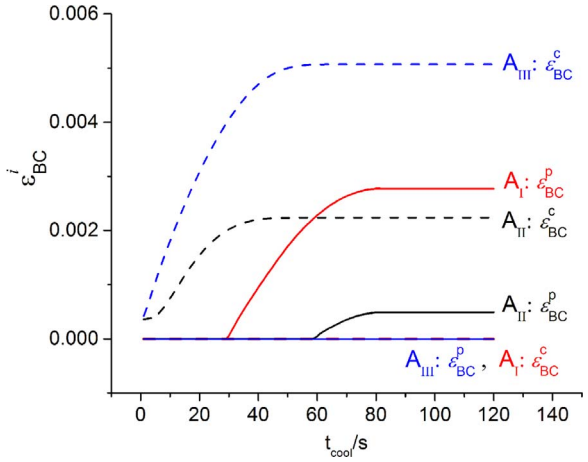

Fig. 5. Evolution of the maximum equivalent creep and plastic strain of BC during cooling.

the accumulation of the stresses caused by the CTE (thermal expansion coefficient) mismatch between the layers, while no creep occurs (see Fig. 5). Thus, the stress in this section is mainly affected by the CTE mismatch of layers and the plastic deformation. So the interface stresses stay unchanged for different BC creep rates in Section 1; at the same time, the maximum tensile stress locates at the TC valley and BC peak (Fig. 3), which indicates that cracks may happen at these locations during cooling. In Section 2 with medium creep rates (A_{BC} = 10^{-2}–1 $MPa^{-4.1}$ s^{-1}), both the creep and plastic deformations take place. The cooling stresses are now relaxed partly by creep. However, the stresses are still large enough to induce plastic deformation. The creep and plastic deformations, as well as the CTE mismatch, dominate the stress development. The maximum tensile stress on the TC interface now deviates from the valley (Fig. 3(a)). The reason is that, larger creep rate leads to the more obvious creep relaxation effect, which can reduce the plastic zone at the BC valley. It enhances the deformation resistance of BC at the valley and suppresses out-of plane displacement of TGO. Consequently, the maximum tensile stress moves to the protuberance of the interface, and cracks may happen here in Section 2. Meanwhile, the stresses on BC-TGO interface decrease slightly due to the creep relaxation (Fig. 3(b)). In Section 3 with larger creep rates (A_{BC} = 1–10^5 $MPa^{-4.1}$ s^{-1}), the cooling stresses can be relaxed by the creep at the beginning of the cooling stage, which are not large enough to induce BC yield. Thus, there exists no plastic deformation but only the creep deformation in this section (Fig. 5), and creep is the main factor affecting the stress development. And the stresses in BC are mostly relaxed. The maximum equivalent creep strain appears at the BC valley (Fig. 6), where the BC layer imposes significant effects of pulling the TC layer at the valley. This effect becomes more prominent with the creep rate increasing, leading to the maximum stress on TC interface moving back to the valley, shown in Fig. 3(a).

4.2. The effects of TGO creep-plastic behavior on the stress development

In this part, the effects of TGO creep-plastic behavior on the stress development are investigated, and the creep-plastic behavior of BC is also considered. Three TGO creep rates are considered, with A_{TGO} valuing 0, 6.8 × 10^8, 6.8 × 10^{13} MPa $^{-4.1}$ s^{-1}respectively.

The stresses at the TC valley and peak, the BC peak are shown in Fig. 7(a) and (b). It can be found that, the creep in TGO tends to reduce the overall stresses in TBCs. In Section 1, the stress at the TC valley is independent of the TGO creep, while the stresses at the TC and BC peaks reduce significantly if the TGO relaxation is enhanced with larger TGO creep rates. When the BC creep rate increases to the values in Section 3, the relaxation effect of the TGO creep on the stress at the BC peak becomes smaller, while the effect on the TC interface becomes larger.

4.3. The effects of TGO thickness on the stress development

As proposed by Bäker et al. [22], the BC and TGO have an opposite effect on the stress state: the BC has a larger CTE than the TC, so a compressive stress state can be induced at the TC valley and tensile at the TC peak; on the other hand, because the CTE of the TGO is smaller than that of the TC, it causes a tensile stress state at the TC valley and compressive at the TC peak. The two opposite effects are therefore called as *BC-induced stresses* and *TGO-induced stresses*, respectively. To investigate detailedly the effects of the *BC-induced* and *TGO-induced* on the stress state, the TGO thickness and non-linear behavior of the BC are considered here. Three TGO thickness h_{TGO} = 2 μm, 4 μm and 6 μm can be obtained if the TBCs are exposed to 1100 °C for 50 h, 150 h and 300 h, respectively.

Fig. 8(a) shows that, with a small TGO thickness h_{TGO} = 2 μm, the BC-induced stresses determine the state, so the stress at the TC valley shows a compressive region in Section 1. As the BC creep rate increases, effect of the BC-induced stresses weakens. Thus the *TGO-induced* stresses dominate, and the stress state then shifts to tensile in Section 3. The stress at the TC peak yet acts oppositely. When the TGO thickens to 4 μm, the TGO-induced stresses mainly affect the state, leading to a tensile state at the TC valley in Section 1. The maximum stress on the TC interface moves from the valley to the middle with the BC creep rate increasing. Thus, the stress state at the TC valley becomes compressive in Section 2, and turns back to tensile in Section 3. If TGO thickens further, the TGO-induced stresses determine the state no matter how large the BC creep rate is, and the stress keeps tensile at the TC valley and compressive at the peak. Fig. 8(b) shows that the stress at the BC peak just increases as the TGO thickens.

4.4. The influence of BC interface roughness on the stress development

The interface becomes rough during the TBCs manufacturing process, and can be facilitated by the compressive stress in TGO

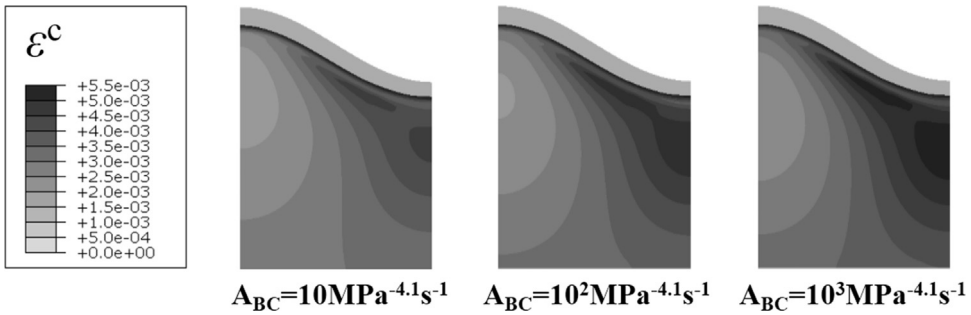

Fig. 6. Contour plots of equivalent creep strain after cooling for different creep rates in Section 3.

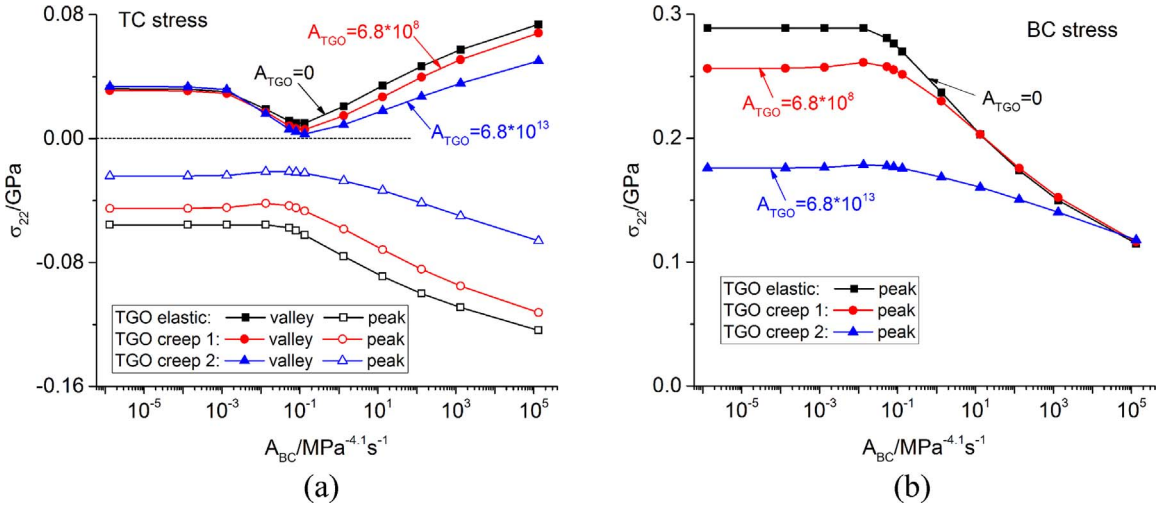

Fig. 7. Stress σ_{22} considering TGO creep-plastic behavior. (a) For the valley and peak positions on TC/TGO interface; (b) for the peak position on BC/TGO interface.

growing. The interface roughness has a strong impact on the stress magnitude and state [33]. In this part, different interface amplitudes are considered with the amplitude a = 6 μm and 24 μm (Fig. 9). Fig. 10(a) and (b) show that with a rougher BC surface, the stresses become higher, leading to a larger equivalent plastic strain (Fig. 11). Additionally, rougher interface can push the maximum tensile stress on the TC/TGO interface (Fig. 10 (a)) towards the middle of the interface. This phenomenon is aggravated in Section 2, and a compressive stress state therefore occurs at the TC valley.

4.5. The stress evolution at different cooling rates

Several cooling stages have been generally considered in previous research, such as a cooling stage for 120 s, 10 min and 30 min [11,34]. This section aims to explore the influence of cooling rate on the creep evolution and stress development during the cooling stage.

The BC is assumed to be creep-plastic and TGO elastic. After exposure at 1100 °C, the TBCs cool to 20 °C in 120 s, 1200 s and 1800 s, respectively. The creep evolutions during cooling are shown in Fig. 12. It can be found that creep process can be significantly affected by the cooling rate. With a higher cooling rate, the equivalent creep strain of BC becomes larger, which can increase the stresses on TC interface while decrease the stresses on BC interface, as shown in Fig. 13.

5. Conclusions

Considering the non-linear creep and plastic behaviors simultaneously, this work investigates the evolution of the creep and plastic deformations, and the stress development when considering creep-plastic behavior of BC and TGO during cooling.

For the first time, three sections are identified in the evolution of creep and plastic deformations if the BC creep rate varies in wide margins:

- Section 1 is a plasticity range with a small BC creep rate, in which the plastic deformation mainly affects the stress state.
- In Section 2, the creep and plastic deformations co-exist, affecting the stress state together. The maximum tensile stress on TC interface moves from the valley towards the middle of the interface. Thus, failure may occur at middle of the interface.
- Section 3 is a creep-controlled range. Stresses are significantly affected by the BC creep in this section: the creep in BC tends to increase the TC stresses, yet reduce the BC stresses.

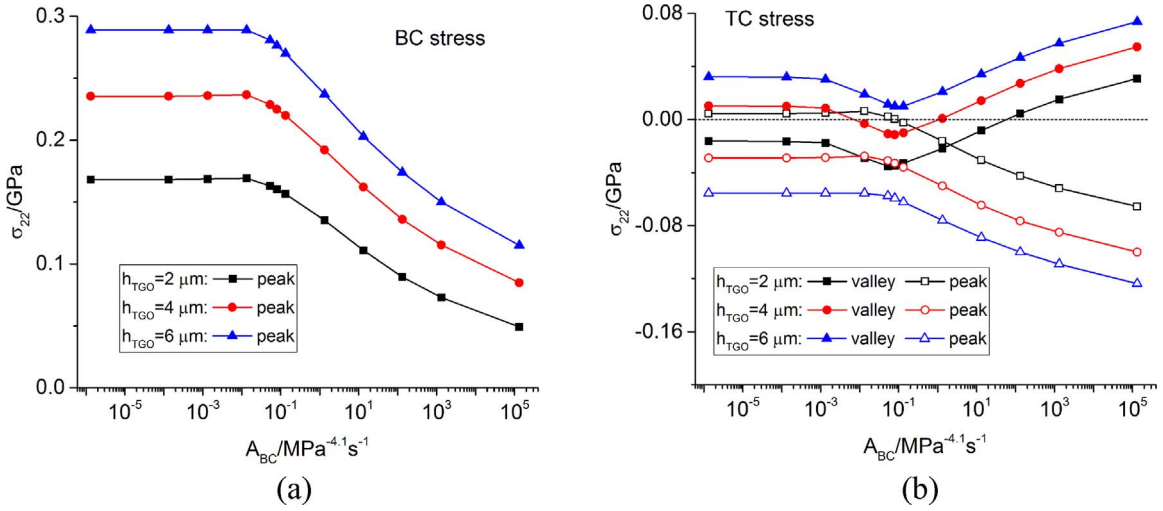

Fig. 8. Stresses σ_{22} for different TGO thickness. (a) For the valley and peak positions on TC/TGO interface; (b) for the peak position on BC/TGO interface.

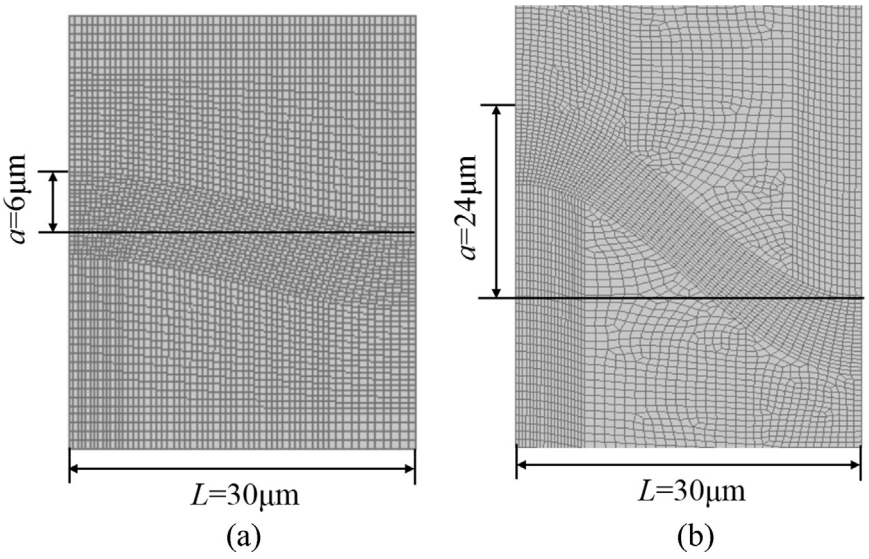

Fig. 9. Interface morphologies applied in this part. (a) a/L = 0.2; (b) a/L = 0.8.

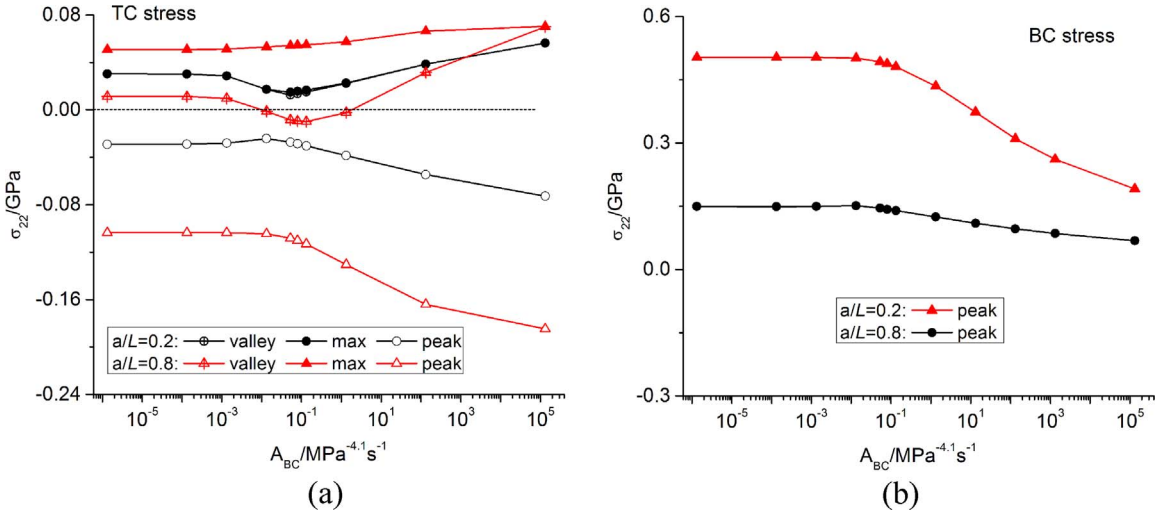

Fig. 10. Stress σ_{22} for different interface roughness ratios. (a) For the maximum stress, the valley and peak positions on TC/TGO interface; (b) for the peak position on BC/TGO interface.

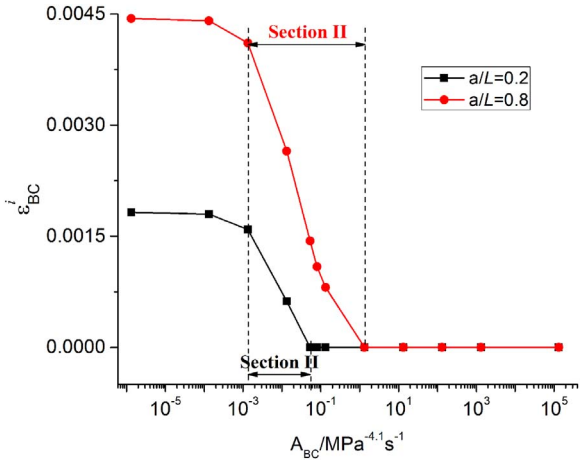

Fig. 11. Evolution of the maximum equivalent plastic strain for different interface roughness ratios.

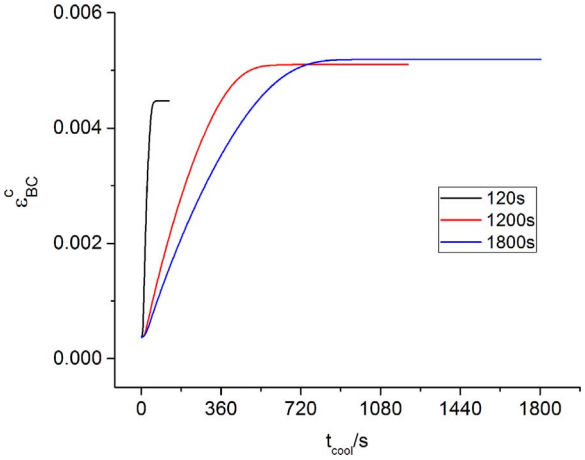

Fig. 12. The maximum equivalent creep strain of BC during cooling for different cooling rates.

Throughout the three sections, both plastic and creep can affect the stress state in TBCs, while the creep is the main process relaxing the stresses. If the creep in TGO is considered, the stresses are overall relaxed no matter if BC is plastic, creep or creep-plastic material.

At last, the effects of TGO growth, geometry morphology and cooling rate on the stress development are also discussed:

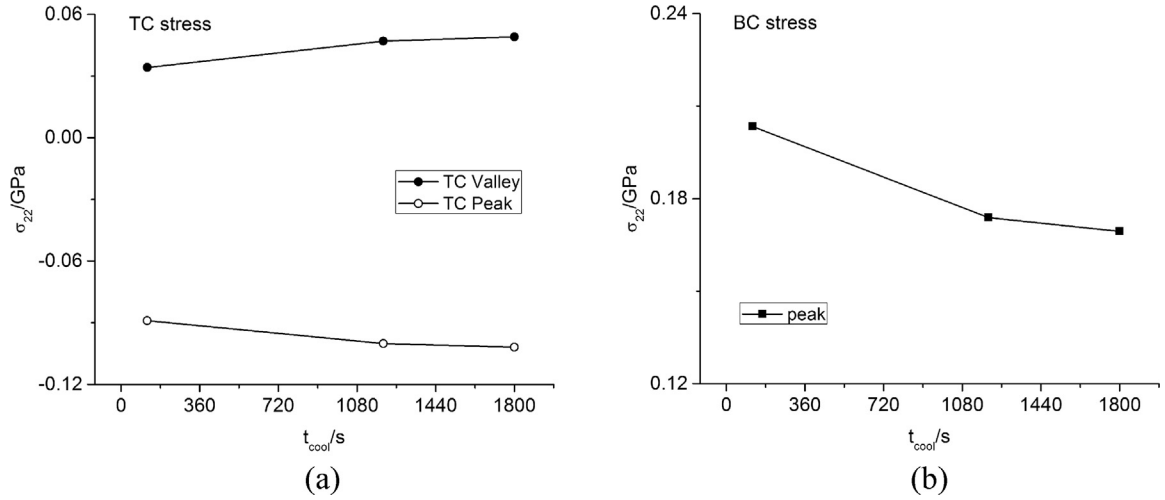

Fig. 13. Stresses σ_{22} for different cooling rates. (a) For the valley and peak positions on TC/TGO interface; (b) for the peak position on BC/TGO interface.

- With different BC creep rates, the effects of TGO thickness on the stress state of TC/TGO interface are different. In Section 1 with small creep rates, the final stress state on the TC/TGO interface can be changed between compressive and tensile as TGO thickens, which possibly induces cracks. The same phenomenon can be found in Section 2. In Section 3 with larger creep rates, the stress magnitude rather than the stress state changes with TGO growing.
- Larger interface roughness can increase the stresses, and push the maximum tensile stress towards the middle of the interface.
- Cooling rate affects the creep process obviously. A low cooling rate can increase the effect of creep on the interface stresses.

Acknowledgement

This work is supported by the National Natural Science Foundation of China (No. 11472206) and the National Basic Research Program of China (No. 2013CB035704).

References

[1] D.R. Clarke, S.R. Phillpot, Thermal barrier coating materials, Mater. Today 8 (2005) 22–29.
[2] D.R. Clarke, M. Oechsner, N.P. Padture, Thermal barrier coatings for more efficient gas-turbine engines, MRS Bull. 37 (2012) 891–898.
[3] N.P. Padture, M. Gell, E.H. Jordan, Thermal barrier coatings for gas-turbine engine applications, Science 296 (2002) 280–284.
[4] T.M. Pollock, D.M. Lipkin, K.J. Hemker, Multifunctional coating interlayers for thermal-barrier systems, MRS Bull. 37 (2012) 923–931.
[5] W. Beele, G. Marijnissen, A. van Lieshout, The evolution of thermal barrier coatings-status and upcoming solutions for today's key issues, Surf. Coat. Technol. 120 (1999) 61–67.
[6] A. Feuerstein, J. Knapp, T. Taylor, A. Ashary, A. Bolcavage, N. Hitchman, Technical and economical aspects of current thermal barrier coating systems for gas turbine engines by thermal spray and EB-PVD: a review, J. Therm. Spray Tecnol. 17 (2007) 199–213.
[7] A. Rabiei, A.G. Evans, Failure mechanisms associated with the thermally grown oxide in plasma-sprayed thermal barrier coatings, Acta Mater. 48 (2000) 3936–3976.
[8] K.W. Schlichting, N.P. Padture, E.H. Jordan, M. Gell, Failure modes in plasma-sprayed thermal barrier coatings, Mater. Sci. Eng. A 342 (2003) 120–130.
[9] M. Martena, D. Botto, P. Fino, S. Sabbadini, M.M. Gola, C. Badini, Modeling of TBC system failure: stress distribution as a function of TGO thickness and thermal expansion mismatch, Eng. Fail. Anal. 13 (2006) 409–426.
[10] A.G. Evans, D.R. Clarke, C.G. Levi, The influence of oxides on the performance of advanced gas turbines, J. Eur. Ceram. Soc. 28 (2008) 1405–1419.
[11] E.P. Busso, J. Lin, S. Sakurai, A mechanistic study of oxidation-induced degradation in a plasma-sprayed thermal barrier coating system: part I: model formulation, Acta Mater. 49 (2001) 1515–1528.
[12] A.M. Freborg, B.L. Ferguson, W.J. Brindley, G.J. Petrus, Modeling oxidation induced stresses in thermal barrier coatings, Mater. Sci. Eng. A 245 (1998) 182–190.
[13] J. Rösler, M. Böker, M. Volgmann, Stress state and failure mechanisms of thermal barrier coatings: role of creep in thermal grown oxide, Acta Mater. 49 (2001) 3659–3670.
[14] J.A. Thompson, T.W. Clyne, The effect of heat treatment on the stiffness of zirconia top coats in plasma-sprayed TBCs, Acta Mater. 9 (2001) 1565–1575.
[15] A. Cipitria, I.O. Golosnoy, T.W. Clyne, A sintering model for plasma-sprayed zirconia TBCs. Part I: free-standing coatings, Acta Mater. 57 (2009) 980–992.
[16] B.W. Lv, H. Xie, R. Xu, X.L. Fan, W.X. Zhang, T.J. Wang, Effects of sintering and mixed oxide growth on the interface cracking of air-plasma-sprayed thermal barrier coating system at high temperature, Appl. Surf. Sci. 360 (2016) 461–469.
[17] M. Bäker, J. Rösler, E. Affeldt, The influence of axial loading on the interface stresses of thermal barrier coatings, Comput. Mater. Sci. 47 (2009) 466–470.
[18] Y.J. Chai, C. Lin, Y.M. Li, Study on stress development in the phase transition layer of thermal barrier coatings, Materials 9 (2016) 773.
[19] M.Y. He, J.W. Hutchinson, A.G. Evans, Simulation of stresses and delamination in a plasma-sprayed thermal barrier system upon thermal cycling, Mater. Sci. Eng. A 345 (2003) 172–178.
[20] E.P. Busso, Z.Q. Qian, M.P. Taylor, H.E. Evans, The influence of bondcoat and topcoat mechanical properties on stress development in thermal barrier coating systems, Acta Mater. 57 (2009) 2349–2361.
[21] J. Rösler, M. Bäker, K. Aufzug, A parametric study of the stress state of thermal barrier coatings part I: creep relaxation, Acta Mater. 52 (2004) 4809–4817.
[22] M. Bäker, J. Rösler, G. Heinze, A parametric study of the stress state of thermal barrier coatings part II: cooling stresses, Acta Mater. 53 (2005) 469–476.
[23] M. Ranjbar-Far, J. Absi, G. Mariaux, F. Dubois, Simulation of the effect of material properties and interface roughness on the stress distribution in thermal barrier coatings using finite element method, Mater. Des. 31 (2010) 772–781.
[24] H.J. Frost, M.F. Ashby, Deformation Mechanism Maps: the Plasticity and Creep of Metals and Ceramics, Pergamon Press Ltd., New York, 1982.
[25] P. Seiler, M. Bäker, J. Rösler, Multi-scale failure mechanisms of thermal barrier coating systems, Comput. Mater. Sci. 80 (2013) 27–34.
[26] C. Lin, Y.M. Li, Stress evolution considering the combined creep-plastic behavior in thermal barrier coatings, Mater. Des. 89 (2016) 245–254.
[27] H.E. Evans, Stress effects in high-temperature oxidation of metals, Int. Mater. Rev. 40 (1995) 1–40.
[28] J. Skrzypek, Plasticity and Creep. Theory, Examples and Problems, CRC Press Inc., Boca Raton, 1993.
[29] T.S. Hille, S. Turteltaub, A.S.J. Suiker, Oxide grown and damage evolution in thermal barrier coatings, Eng. Fract. Mech. 78 (2011) 2139–2052.
[30] J. Cheng, E.H. Jordan, B. Barber, M. Gell, Thermal/residual stress in an electron beam physical vapor deposited thermal barrier coating systems, Acta Mater. 46 (1998) 5839–5850.
[31] E.P. Busso, H.E. Evans, Z.Q. Qian, M.P. Taylor, Effects of breakaway oxidation on local stresses in thermal barrier coatings, Acta Mater. 58 (2010) 1242–1251.
[32] P.N. Quested, R.F. Brooks, L. Chapman, R. Morrell, Y. Youssef, K.C. Mills, Measurement and estimation of thermophysical properties of nickel based superalloys, Mater. Sci. Technol. 25 (2009) 154–162.
[33] Q.M. Yu, H.L. Zhou, L.B. Wang, Influences of interface morphology and thermally grown oxide thickness on residual stress distribution in thermal barrier coating system, Ceram. Int. 42 (2016) 8338–8350.
[34] A.M. Karlsson, C.G. Levi, A.G. Evans, A model study of displacement instabilities during cyclic oxidation, Acta Mater. 50 (2002) 1263–1273.